Pergamon

Int. J. Heat Mass Transfer. Vol. 37, No. 12, pp. 1723–1731, 1994
Copyright © 1994 Elsevier Science Ltd
Printed in Great Britain. All rights reserved
0017–9310/94 $7.00+0.00

0017–9310(93)E0103–N

Radiation heat transfer of a Czochralski crystal growth furnace with arbitrary specular and diffuse surfaces

SHIGENAO MARUYAMA and TOSHIO AIHARA

Institute of Fluid Science, Tohoku University, Aoba-ku, Katahira 2-1-1, Sendai 980, Japan

(*Received* 4 *August* 1993 *and in final for* 2 *December* 1993)

Abstract—A numerical method is presented for predicting radiation heat transfer from axisymmetric bodies consisting of numerous arbitrary ring elements. Each ring element has the combined characteristics of specular and diffuse surfaces. The accuracy of the method was verified using a simple configuration. Good agreement between the present numerical and analytical solutions was obtained, and the effect of specular reflectivity was investigated. As a numerical example, radiation heat transfer of the Czochralski crystal growth apparatus was presented. The effect of specular reflection on temperature distribution on the various surfaces was examined. The present radiation transfer method was combined with the finite element package ABAQUS for conduction analysis, and the effect of specular reflectivity on temperature distribution and surface heat flux was investigated.

1. INTRODUCTION

PRECISION heat-transfer control of Czochralski (CZ) crystal growth furnaces has been in great demand because of recent increases in the diameter and quality of semiconductor crystals. Kotake *et al.* [1] developed a computation system for the combined heat transfer analysis of a CZ furnace using inter-university networks.

Radiation heat transfer is important for the precision heat-transfer control of a CZ furnace. The profile of the furnace is complicated and changes with processing time. Accordingly, applying a radiation heat-transfer analysis for a simple configuration is difficult. Several existing studies [2–5] have been done on radiation heat transfer of CZ furnaces; however, these are applicable only when the surfaces are diffuse.

Surfaces are not always diffuse, but may be specular or have a combination of specular and diffuse characteristics. The surfaces of silicon solid and melt are generally specular, and metal vessels containing the furnace are usually specular. The existing radiation analysis for diffuse surfaces may contain substantial error, and precise estimation of radiation flux and temperature on the specular surfaces is difficult. There have been methods for radiation heat transfer between specular surfaces proposed by Sparrow *et al.* [6] and Masuda [7]; however, these are restricted only for very simple configurations in practical applications.

Recently, the finite element method (FEM) and boundary element method (BEM) have become popular tools for computer aided engineering (CAE). These methods can be applied to almost any geometrical configuration by a single computer program without any special knowledge, such as that required for taking pictures by an idiot camera. Also recent improvements in computer technology enable us to treat a large matrix calculation.

The authors presented a simple numerical method for analyzing radiative transfer from three-dimensional bodies of arbitrary configuration, and proposed an effective radiative exchange area for simplifying the analysis [8]. One of the authors introduced a new definition of absorbing and diffuse reflection view factors for analyzing radiative transfer of three-dimensional arbitrary bodies with specular and diffuse surfaces. The bodies comprise numerous polygons, and temperature or heat flux is arbitrarily specified on each surface [9].

The above-mentioned three-dimensional method can be applied to axisymmetric bodies. However, the calculation time needed is proportional to the square of the number of total surface elements. Consequently, the efficiency of calculation is extremely low if one constructs an analysis model from three-dimensional polygons.

In the present study, we propose a new calculation method applicable to arbitrary axisymmetric bodies consisting of numerous ring elements. The accuracy of the present method was compared with analytical solutions using a simple configuration, and the effect of specular reflection on heat transfer characteristics was investigated.

Finally radiation heat transfer of a CZ crystal growth furnace was investigated and the effect of specular reflectivity was estimated. The present method of radiation heat transfer was combined with the finite element package ABAQUS for conduction analysis. The effect of specular and diffuse reflection

NOMENCLATURE

A_i	surface element or area of the element
$F_{i,j}$	view factor from element A_i to A_j
$F_{i,j}^{A}$	absorption view factor, equation (3)
$F_{i,j}^{D}$	diffuse reflection view factor, equation (4)
$\mathbf{F}$	view factor matrix
G_i	irradiance
n_θ, n_ϕ	partition number of rays in θ and ϕ directions
n_p	partition number of a surface
N	total number of surface elements
q_X^*	dimensionless heat fluxes, Q_X/Q_T
Q_T	heat transfer rate of thermal emission, $A_i\varepsilon\sigma T_i^4$, Fig. 1
Q_X	heat transfer rate of net heat loss, Fig. 1
$\mathbf{Q}$	heat transfer rate vector
T_i	surface temperature
x, z	coordinates in radial and axial directions, Fig. 2.

Greek symbols

α, ε	absorptivity and emissivity
ΔF	numerical error of a view factor, equation (18)
θ	polar angle measured from normal vector of a surface
ρ^D	diffuse reflectivity
ρ^S	specular reflectivity
σ	Stefan–Boltzmann constant
ϕ	circumferential angle.

Subscripts

i, j	values on surface element A_i and A_j, respectively
T, X	values due to thermal emission and net heat loss.

on the surface heat flux and temperature distribution was investigated.

2. METHOD OF ANALYSIS

2.1. *Absorption and diffuse reflection view factors*

Radiation heat transfer between surfaces in non-participating media is a classical problem. Most of the analyses assumed a gray and diffusely emitting and reflecting surface, and introduced the view factor of a surface element A_i as follows:

$$F_{i,j} = \frac{1}{A_i}\int_{A_i}\int_{A_j}\frac{\cos\theta_i\cos\theta_j}{\pi r^2}\,\mathrm{d}A_i\,\mathrm{d}A_j \qquad (1)$$

where r is the distance between elements $\mathrm{d}A_i$ and $\mathrm{d}A_j$. The above expression for the view factor is a geometrical function of only the relative positions of surface elements. The analytical procedure for obtaining the view factor is simplified; however, radiation transfer using the view factor in equation (1) becomes very complicated [9] when the system includes specular surfaces or specular and diffuse surfaces, as shown in Fig. 1.

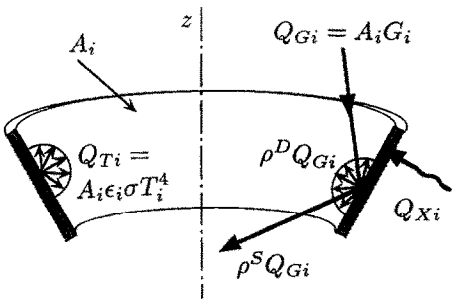

FIG. 1. A ring element with a specular and diffuse surface and heat balance of radiation and net heat loss.

The basic definition or physical meaning of the view factor is introduced in the present study. Then, an absorption view factor $F_{i,j}^{A}$ and a diffuse reflection view factor $F_{i,j}^{D}$ are introduced as follows:

$F_{i,j}^{A}$: the fraction of the radiation leaving surface element A_i that is absorbed by surface A_j.
$F_{i,j}^{D}$: the fraction of the radiation leaving surface element A_i that is diffusely reflected by surface A_j.

Since a fraction of the specular reflection is either absorbed or diffusely reflected by other surface elements after several specular reflections, the specular fraction is not added to the view factors. The ray emitted from A_i may be reabsorbed by the same element A_i after specular reflections on the other elements.

In order to simplify the problem, the following assumptions are introduced.

(1) Each surface element has constant temperature, heat flux and emissivity over the surface element.

(2) The surface is gray and opaque against thermal radiation.

(3) The reflectivity and emissivity of a surface element are independent of the incident angle, as shown in Fig. 1.

The reflectivity and emissivity are not constant on actual surfaces near $\theta = \pi/2$. However, the effect of the dependence on heat transfer is considered to be small because of the nature of the cosine law of the emission. Silicon crystal at room temperature is transparent against radiation whose wavelength is larger than 1.1 μm. However, high-temperature silicon solid and melt can be treated as opaque against thermal radiation [10]. In general, reflectivity of a solid surface is dependent on the wavelength. However, the spec-

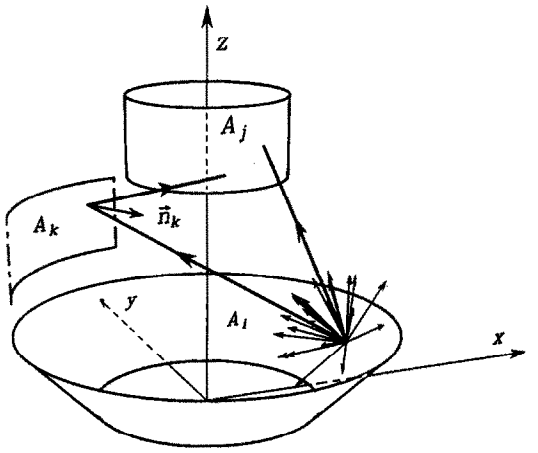

FIG. 2. Analysis model of arbitrary ring elements and emission of radiation.

tral dependence is not so critical in the visible and infrared regions compared with that of absorption coefficient and emissivity of gas. Consequently, it is considered that the assumption (2) gives reasonable approximation in the present case.

According to the assumptions and referring to Fig. 1, the reflectivity of element A_i is divided by the two components of diffuse and specular reflectivity as follows:

$$\rho_i = \rho_i^{\mathrm{S}} + \rho_i^{\mathrm{D}} = 1 - \alpha_i = 1 - \varepsilon_i. \tag{2}$$

Considering equation (2) and the definition of view factors, $F_{i,j}^{\mathrm{A}}$ and $F_{i,j}^{\mathrm{D}}$ can be written as follows:

$$F_{i,j}^{\mathrm{A}} = \frac{1}{\pi A_i}\int_{A_i}\int_{h} f_i^j(\theta,\phi)\varepsilon_j \cos\theta \,\mathrm{d}\omega \,\mathrm{d}A_i \tag{3}$$

$$F_{i,j}^{\mathrm{D}} = \frac{1}{\pi A_i}\int_{A_i}\int_{h} f_i^j(\theta,\phi)\rho_j^{\mathrm{D}} \cos\theta \,\mathrm{d}\omega \,\mathrm{d}A_i \tag{4}$$

where $\int_h \mathrm{d}\omega$ expresses integration over the hemispherical solid angle, and $f_i^j(\theta,\phi)$ is the fraction of the ray emitted from $\mathrm{d}A_i$ in the direction of (θ,ϕ) that is intercepted by A_j. As shown in equations (3) and (4) and Fig. 2, the present view factor is a function not only of the geometrical configuration, but also of emission and reflection characteristics.

2.2. *Calculation of view factors*

Recent progress in computer graphics has accelerated improvement in the ray tracing method for visualizing calculated data. A radiation ray tracing method has been used for analyzing the directional emission characteristics of an involute reflector [11]. The radiation ray tracing method can result in a substantial saving of calculation time [12] compared with the Monte Carlo method. In the present analysis, the radiation ray tracing method is adopted for estimating the absorption view factors and the diffuse reflection view factors discussed in the previous section.

An analysis model for the present axisymmetric system is shown in Fig. 2. Arbitrary bodies are constructed by numerous ring elements i $(i = 1,..,N)$. These elements are parts of a circular disc, cylinder or cone, and expressed as follows:

$$\left.\begin{array}{rl} & a(x^2+y^2)+b(z-c)^2 = d \\ \text{Circular disk:} & a = 0, d = 0, \\ \text{Cylinder:} & b = 0, \\ \text{Cone:} & d = 0, a > 0, b < 0 \end{array}\right\}. \tag{5}$$

Consider a crosssection of a ring element in the x–z plane, and let the start and end points be s_1 and s_2, respectively. The surface area of element i and the centroid is expressed by the following relations.

$$A_i = 2\pi\int_{s_1}^{s_2} x \,\mathrm{d}s \tag{6}$$

$$x_{ci} = \int_{s_1}^{s_2} x^2 \,\mathrm{d}s \Big/ \int_{s_1}^{s_2} x \,\mathrm{d}s \tag{7}$$

where s is a distance along the element in the x–z plane.

The radiation energy is emitted from the centroid of element A_i, and is divided into $(1+n_\theta n_\phi)$ bundles of rays whose initial intensity is $1/(1+n_\theta n_\phi)$. The initial direction (θ_i, ϕ_j) of the ray is expressed as follows.

$$\left.\begin{array}{l} \theta_1 = \phi_1 = 0 \\ \theta_i = \{\sin^{-1}[(1+in_\phi - n_\phi)/(n_\phi n_\theta + 1)]^{0.5} \\ \qquad +\sin^{-1}[(1+in_\phi)/(n_\phi n_\theta + 1)]^{0.5}\}/2 \\ \phi_j = 2\pi(j-1)/n_\phi, \quad \text{for } (i \neq 1, j \neq 1) \end{array}\right\}. \tag{8}$$

The rays emitted from A_i according to equation (8) are shown in Fig. 2, for the case of $n_\theta = 3$, $n_\phi = 7$. Each ray has uniform intensity, and angular density of emission is high near the normal direction.

The pencil of the ray is traced numerically according to the following process:

(1) When the ray emitted from element A_i strikes surface A_j, the intensity of the ray is divided into the absorbed fraction $\mathrm{d}I^{\mathrm{A}}$, diffusely reflected fraction $\mathrm{d}I^{\mathrm{D}}$, and specular reflected fraction $\mathrm{d}I^{\mathrm{S}}$ according to equation (2).

(2) Then, $\mathrm{d}I^{\mathrm{A}}$ and $\mathrm{d}I^{\mathrm{D}}$ are added to $F_{i,j}^{\mathrm{A}}$ and $F_{i,j}^{\mathrm{D}}$, respectively, and the reflected ray with intensity $\mathrm{d}I^{\mathrm{S}}$ is traced again.

(3) When the ray strikes the surface $A_{j'}$, the absorbed and diffusely reflected portions are added to $F_{i,j'}^{\mathrm{A}}$ and $F_{i,j'}^{\mathrm{D}}$, respectively, and the specular fraction is traced again until the ray is attenuated to less than 1% of its initial strength or absorbed completely. Note that the specular fraction of the ray carries with it the information on the intensity and the element i from which the ray was originally emitted; however, the ray is oblivious to the procedure by which element the ray was reflected. It should be noted that the model is axisymmetric; however, the ray tracing should be carried out in a completely three-dimensional system. Otherwise, the tracing of a skew ray cannot be treated

properly, and the analysis may cause a substantial error.

After tracing the rays from all the surface elements, $F^{A}_{i,j}$ and $F^{D}_{i,j}$ can be obtained automatically. It should be noted that the ray tracing method described above is not only suitable for a supercomputer with a vector processor, but is also effective for computers with parallel processors because the procedure can be performed independently.

2.3. *Radiation transfer*

For analyzing radiation heat transfer between specular and diffuse surfaces, the diffuse radiosity J_{Di} is defined as follows:

$$J_{Di} \equiv \varepsilon_i \sigma T_i^4 + \rho_i^{D} G_i \tag{9}$$

where G_i is the irradiance on surface A_i. The diffuse radiation heat transfer rate Q_{Ji} is expressed as

$$Q_{Ji} \equiv A_i J_{Di} = A_i(\varepsilon_i \sigma T_i^4 + \rho_i^{D} G_i). \tag{10}$$

The net rate of heat loss Q_{Xi} can be derived from the heat balance on surface A_i, as shown in Fig. 1,

$$Q_{Xi} = A_i \varepsilon_i (\sigma T_i^4 - G_i). \tag{11}$$

Consider the closed enclosure system composed of N surface elements. Defining the irradiation energy and emissive power on element A_i as $Q_{Gi} \equiv A_i G_i$ and $Q_{Ti} \equiv A_i \varepsilon_i \sigma T_i^4$, and using $F^{D}_{i,j}$ and $F^{A}_{i,j}$ from the previous section, the irradiation energy and absorption energy can be expressed as follows:

$$\rho_i^{D} Q_{Gi} = \sum_{j=1}^{N} F^{D}_{j,i} Q_{Ji} \tag{12}$$

$$A_i \varepsilon_i G_i = \sum_{j=1}^{N} F^{A}_{j,i} Q_{Jj}. \tag{13}$$

Hence, equations (10) and (11) can be rewritten as follows:

$$Q_{Ji} = Q_{Ti} + \sum_{j=1}^{N} F^{D}_{j,i} Q_{Jj} \tag{14}$$

$$Q_{Xi} = Q_{Ti} - \sum_{j=1}^{N} F^{A}_{j,i} Q_{Jj}. \tag{15}$$

If we express $F_{j,i}$ as matrix $\mathbf{F}$ and Q_i as vector $\mathbf{Q}$, and eliminate Q_{Ji} from equations (14) and (15), the following relationship can be obtained:

$$\mathbf{F_X Q_T} = \mathbf{I Q_X} \tag{16}$$

where

$$\mathbf{F_X} = \mathbf{I} - \mathbf{F^A}(\mathbf{I} - \mathbf{F^D})^{-1} \tag{17}$$

and $\mathbf{I}$ and $(\,)^{-1}$ are the unit matrix and inverse matrix, respectively. Consider the case when each element is specified temperature T_i or heat flux q_{Xi}; the unknown components of q_{Xi} or T_i are obtained, respectively, by solving equation (16). Details of the numerical processes were described in the previous report [9].

Introducing the rate of heat transfer vector $\mathbf{Q}$, instead of usual heat flux q_i and temperature T_i, and introducing $\mathbf{F^D}$ and $\mathbf{F^A}$, the analysis from equation (16)–(21) becomes purely algebraic. Therefore, the numerical procedure can be simplified, and the conventional algebraic tools for a computer can be easily utilized.

3. RADIATIVE TRANSFER OF A SIMPLE CONFIGURATION

3.1. *View factor*

The present radiation ray tracing analysis for obtaining view factors was applied to a simple configuration, as shown in Fig. 3. The round container is composed of a circular disk #1 and a hollow cylinder #2. The radius of the disk and the height of the cylinder are unity.

The view factor from differential area dA_1 to A_2, $F_{d1,2}$, was calculated for various numbers of ray partitions n_ϕ, n_θ. The analytical solution of the view factor $(F_{d1,2})_a$ was obtained analytically [13]. The numerical error is expressed by the following relationship.

$$\Delta F_{d1,2} \equiv F_{d1,2}/(F_{d1,2})_a - 1. \tag{18}$$

$\Delta F_{d2,1}$ can be defined in a similar manner. Figure 4 shows the accuracy of $F_{d1,2}$ and $F_{d2,1}$ when $n_\phi = n_\theta$. The abscissa expresses the position of dA_1 and dA_2 along the x and z axes. The accuracy of the view factors improves gradually with increasing n_ϕ and n_θ. However, the calculation time increases almost linearly with $n_\phi \times n_\theta$. Therefore, a compromise must be made between accuracy and calculation time. In the present case, sufficient accuracy is obtained for $n_\phi = n_\theta \geqslant 40$, and $n_\phi = n_\theta = 40$ was chosen for the following calculation. The accuracy of the view factors was discussed in detail elsewhere [14].

3.2. *Heat transfer*

In order to investigate the effect of element size on the accuracy of radiation heat transfer, the radiation exchange of the configuration, as shown in Fig. 3, was calculated using the present numerical method. Each panel was divided into n_p elements. Constant temperature is assumed on the surfaces, and the ambient

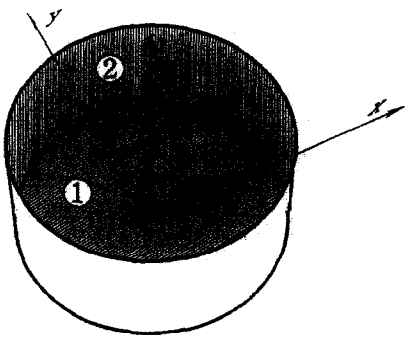

FIG. 3. Radiation model of a simple configuration consist of a disk and a cylinder.

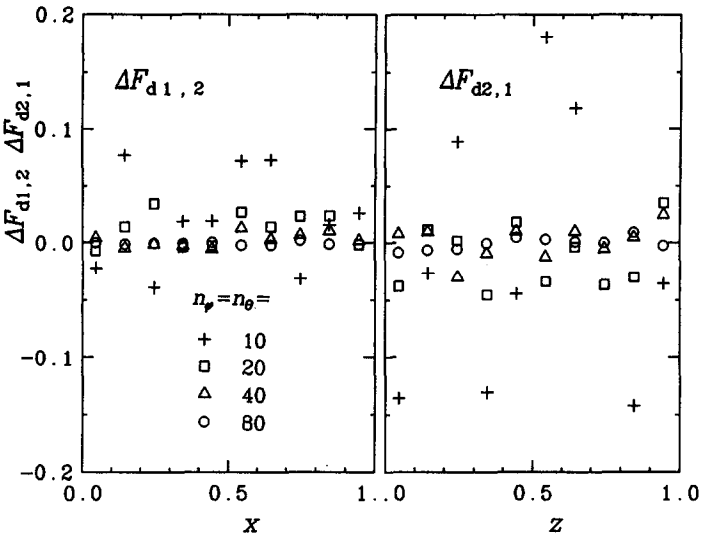

FIG. 4. Accuracy of $F_{d1,2}$ and $F_{d2,1}$ for various ray partitions when $n_\phi = n_\theta$.

is assumed to be black and 0 K. The emissivity on the panel and ambient is unity. The outer surfaces in Fig. 3 are assumed to be adiabatic.

Figure 5 shows the distribution of the net radiative heat flux along the surface elements for various partition numbers n_p. The net rate of heat transfer Q_X is expressed in dimensionless form q_X^*, because the system is linear against Q_T.

The solid line in Fig. 5 is a semi-analytical solution obtained as follows. Each surface element #1 and #2 was divided into 100 zones ($n_p = 100$). Then, the view factors $F_{i,j}$ were obtained analytically [13]. Radiation heat transfer was obtained in the same manner explained in Section 2.3. It is noted that the semi-analytical method is only applicable for diffuse surfaces. Therefore, the specular reflectivity is set to zero in the present numerical simulation, and the numerical results were compared with the semi-analytical solutions.

The numerical solutions with small partition number show relatively good agreement with semi-analytical solutions independent of the partition number. The case of $n_p = 1$, still, shows reasonable agreement with the semi-analytical solution without divergence or any numerical instability. These characteristics are similar to FEM or BEM, and are important for the analysis of arbitrary configuration.

3.3. *Effect of specular reflectivity*

Radiation heat exchange of the configuration in Fig. 3 was calculated for various specular and diffuse reflectivities. The emissivity is fixed at 0.1, and the specular reflectivity was changed from 0 to 0.9. The dimensionless net heat flux q_X^* along the surfaces of a

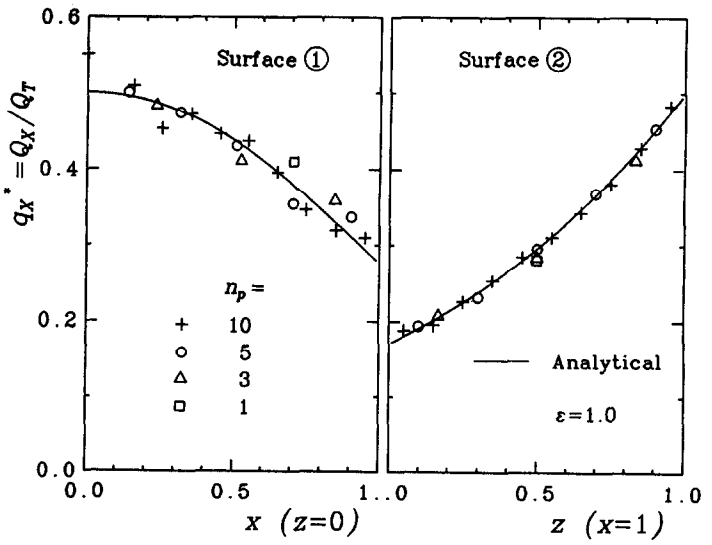

FIG. 5. Effect of element size on accuracy of radiation heat transfer between diffuse surfaces.

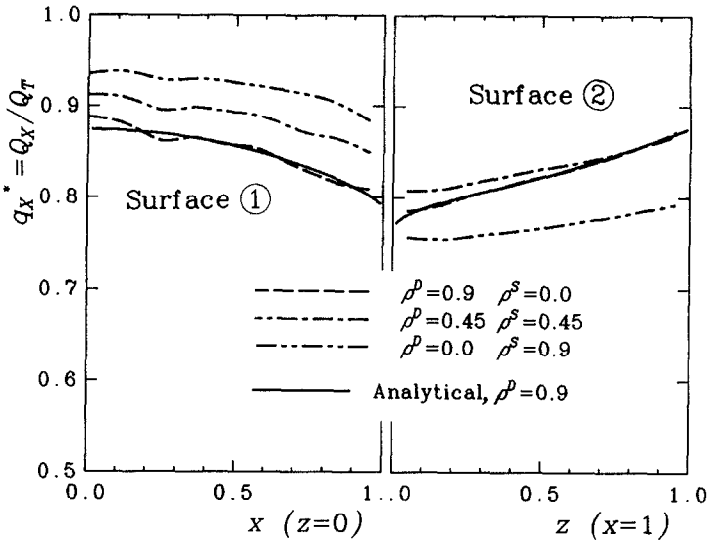

FIG. 6. Effect of specular reflectivity on net heat flux along surfaces 1 and 2 (constant temperature).

constant temperature channel is shown in Fig. 6. The semi-analytical solution explained in the previous section for the diffuse surfaces is also plotted in the figure.

If one compares q_X^* with diffuse and specular surfaces, the value with specular surface is larger than that with diffuse surface on surface #1. The opposite can be seen on surface #2. The flux on surface #2 is maximum for $\rho^D = \rho^S = 0.45$. For a three-dimensional model with unit squares, net heat flux increases monotonously with increasing specular reflectivity [9]. The effect of specular reflectivity for the case of the three-dimensional channel is not as complicated as the present axisymmetric case.

4. RADIATION HEAT TRANSFER OF A CZ CRYSTAL GROWTH FURNACE

4.1. *Analysis model*

The heat transfer analysis model of a Czochralski furnace for silicon crystal growth is shown in Fig. 7. The diameter of the silicon crystal is 250 mm, and the inner diameter of the crucible is 500 mm. Solid silicon in the crucible is assumed in order to simplify the problem. The distance between the top of the crystal and the bottom of the crucible is 525 mm. A graphite heater of 650 mm inner diameter surrounds the crucible. The entire furnace is contained in a metal chamber whose inner diameter is 800 mm and height is 750 mm.

The radiation transfer model composed of ring elements is shown in Fig. 8. The silicon surface is divided into 12 elements. The crucible and heater are divided into 20 and 16 elements, respectively. The total number of ring elements is 88. The emissivity of each surface is specified by Miyahara *et al.* [4]. For the emissivity of the chamber, we adopt the value of stainless steel. Two surface conditions are considered on the silicon surface and the metallic chamber. One is the diffuse case as has been studied by many researchers, and the other is the specular surface with the same emissivity. The value of emissivity and surface conditions are listed in Table 1.

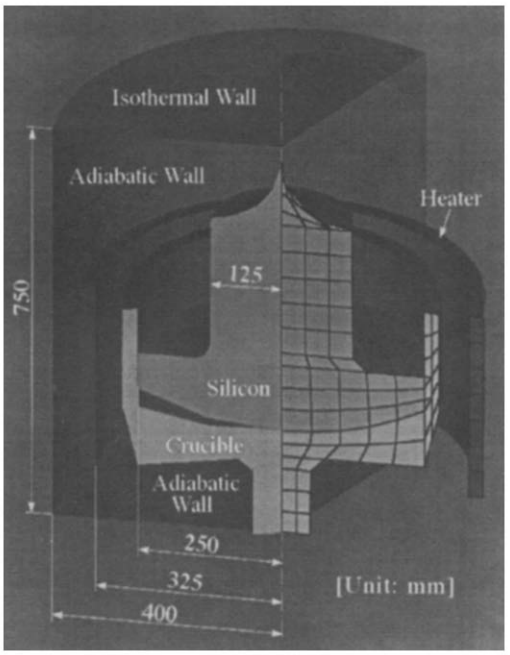

FIG. 7. Combined heat transfer model of radiation and conduction of a Czochralski crystal growth furnace for silicon.

The temperature of the heater is constant at 1000 K. A wide variety of boundary conditions may be considered at the metal chamber. Strictly speaking, one has to take account of the heat transfer on the outer surface of the chamber. For simplicity of the problem, the bottom and side of the chamber are adiabatic, and the top surface is assumed to be at 300 K. These boundary conditions of each surface are indicated in Fig. 8. The ray partition is set at $n_\phi = n_\theta = 80$ for the present model. For generation of

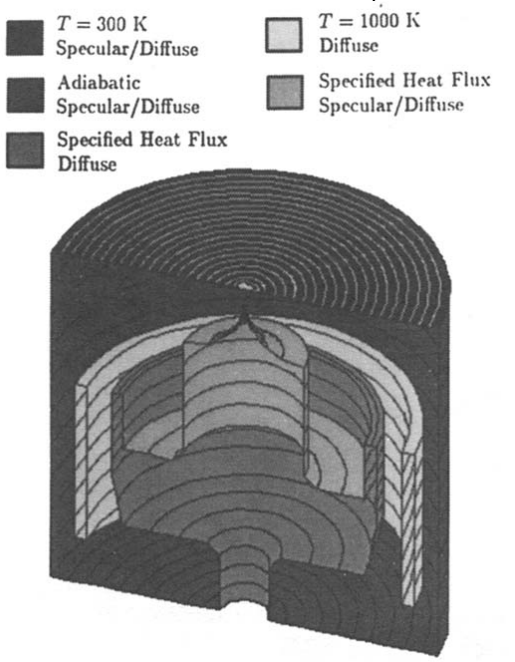

FIG. 8. Boundary condition and surface condition on surface elements.

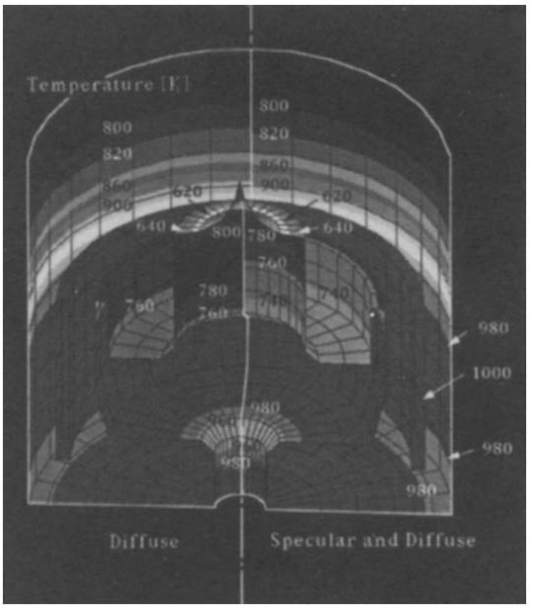

FIG. 9. Temperature distribution on various surfaces of a CZ furnace for the case of adiabatic condition.

coordinate data and presentation of calculated data, the general purpose three-dimensional mechanical CAE software PATRAN was used.

The present method can easily be combined with a calculation package for conduction analysis. The present radiative transfer analysis was combined with a general-purpose finite element analysis program ABAQUS. The converged solution of combined heat transfer was obtained by the iteration process between radiation and conduction analyses. Once the calculation of view factors is completed, the calculation time for obtaining T and Q_X is short. These characteristics of the present analysis are suitable for the iterating process for a given configuration. Total calculation time for the view factors and radiative transfer of the above case was 320 s (for 1 CPU) by CRAY-YMP8/418.

4.2. *Surface temperatures on adiabatic surfaces*

Prior to the analysis of combined heat transfer, radiative transfer of adiabatic surfaces was conducted. The surfaces of the silicon and crucible are assumed to be adiabatic, and surface temperatures are calculated. The temperature distribution of adiabatic surfaces is expressed in three-dimensional form in Fig. 9, and the surface temperatures along the silicon crystal are shown in Fig. 10.

Figure 9 compares the temperature distributions of diffuse surfaces and diffuse and specular surfaces. The temperature on the camber and the outer surfaces of the crucible does not change substantially with surface conditions. However, a marked decrease in temperature with specular surfaces on silicon crystal and the inside wall of the crucible is observed.

The same trend can be seen in Fig. 10, and the specular surfaces represent 30 K lower temperature than the diffuse surface at maximum. The temperature on the shoulder of the crystal (region A) is remarkably low. Discontinuity of temperature at the border between regions A and B is due to the assumption of an adiabatic surface on the crystal. The difference between temperature distributions for the cases of diffuse and specular surfaces is small in region A.

The effect of specular reflectivity is small when the configuration is simple; however, the effect is marked when the shape has a concave part such as regions B and C. This tendency is the same as that in the three-dimensional case [9] investigated on a connecting rod of an automobile. As have been discussed in the Section 3.3, the effect of specular reflectivity on surface temperature and surface heat flux is dependent on the shape of the bodies.

Table 1. Emissivities and surface conditions on the surfaces

Surface	Emissivity	Surface condition
Silicon	0.55	Specular/diffuse
Crucible	0.90	Diffuse
Graphite heater	0.90	Diffuse
Metal chamber	0.50	Specular/diffuse

4.3. *Combined heat transfer model*

Conduction and radiation combined heat transfer analysis of the CZ furnace, as shown in Fig. 7, was conducted. The heat flux and temperature distribution on the surfaces are shown in Fig. 11. The difference in temperature on the crystal between specular and diffuse cases becomes smaller compared with the case

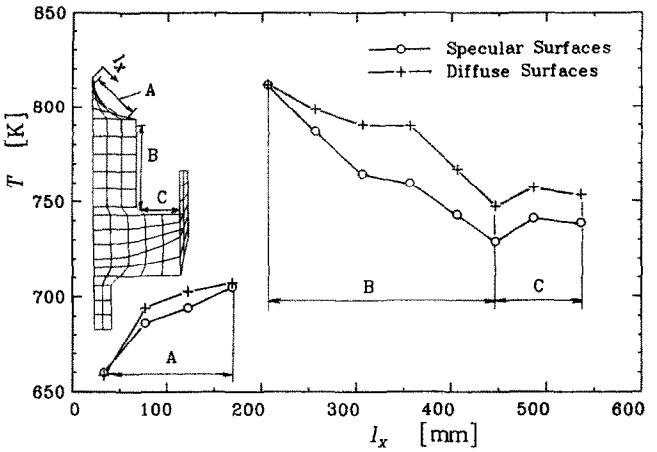

FIG. 10. Temperature distribution along the surface of the silicon crystal for the case of adiabatic condition.

of adiabatic walls. Yet, the specular surface shows lower temperature in regions B and C of Fig. 10. The heat flux on surface elements is shown by arrows in Fig. 11. The heat flux in region B is very small and cannot be expressed in Fig. 11. The flux on regions A and C is large for both diffuse and specular cases. As far as the heat flux is concerned, the effect of specular reflectivity is not very marked.

Temperature distributions in the cross section of the silicon solid and crucible are compared in Fig. 12, for diffuse surfaces and specular and diffuse surfaces. The effect of specular reflectivity is very small in the crucible because the surfaces are diffuse for both cases. However, the temperature distribution in silicon solid with specular surfaces shows a lower value than that with diffuse surfaces. This tendency is marked in the silicon in the crucible and region C of Fig. 10; and the difference in temperature is about 10 K. Due to the effect of conduction, the difference in temperature distribution between specular and diffuse surfaces decreases.

5. CONCLUSIONS

A numerical method was presented for radiation heat transfer of a Czochralski crystal growth furnace. The model consists of numerous arbitrary axisymmetric ring elements; and the temperature condition can be specified arbitrarily on each surface. Each ring element has combined characteristics of specular and diffuse surfaces. The method can be

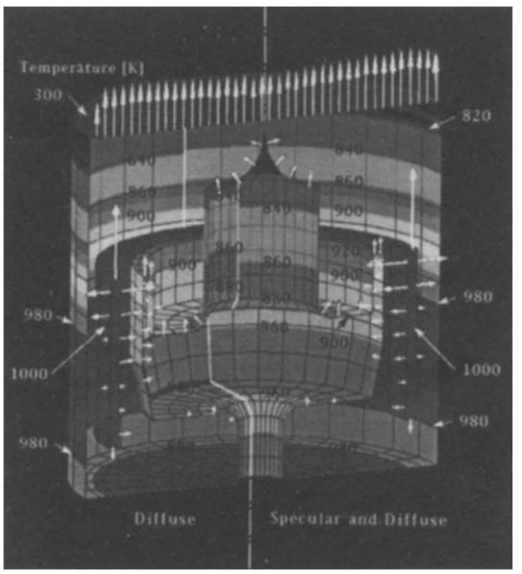

FIG. 11. Temperature distribution and surface heat flux on various surfaces of radiation/conduction combined heat transfer model.

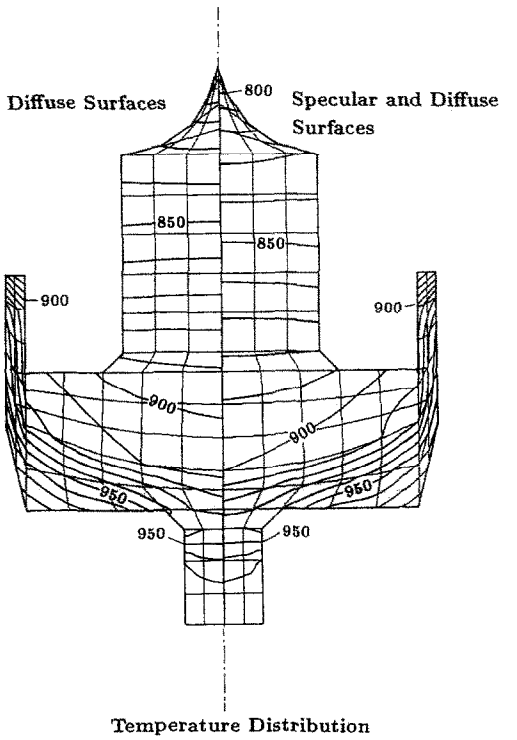

FIG. 12. Temperature distribution in the cross section of silicon crystal of the combined heat transfer model.

easily combined with FEM or other heat transfer analyses.

Its accuracy was verified for a simple configuration, and good agreement with analytical solutions was obtained. The effect of specular reflection on heat transfer was examined using the configuration; the effect depends on the shape of the surface, and is more complicated compared with that of a three-dimensional channel [9].

The heat transfer of the CZ model was investigated for the case of adiabatic surfaces. If specular reflectivity is considered on a metal chamber and silicon surfaces, temperature on the silicon surfaces becomes lower than that when all the surfaces are diffuse. This temperature decrease is marked when the surfaces construct a concave.

The method of radiation heat transfer of the CZ furnace was combined with a general purpose finite element method for conduction heat transfer. The effect of specular reflection on the temperature distribution becomes small compared with the one for adiabatic surfaces. Yet, the temperatures on the specular surfaces and in the cross section of the crystal show lower values than that for the diffuse case. The effect of specular reflection on the surface heat flux is small for the present model.

Acknowledgements—The authors would like to express their gratitude to Mr M. Ukaku of Institute of Fluid Science, Tohoku University, for his assistance in producing graphs. The computations were carried out by CRAY-YMP8/8128 and IRIS-4D/240GTX at the Institute of Fluid Science, Tohoku University. For generating coordinate data and analyzing conduction heat transfer, the general purpose 3-D CAE software package PATRAN and finite element analysis program ABAQUS were used, respectively.

REFERENCES

1. S. Kotake, K. Hijikata, M. Yamada, S. Maruyama, M. Iwamoto and H. Yoshida, Development of a large scale computation system for heat transfer problem by inter-university networks, *Proc. 29th National Heat Transfer Symposium of Japan*, Vol. 1, pp. 376–377. Heat Transfer Society of Japan (1992).
2. F. Dupret, P. Nicodeme, Y. Ryckmans, P. Wouters and M. J. Crochet, Global modeling of heat transfer in crystal growth furnaces, *Int. J. Heat Mass Transfer* **33,** 1849–1870 (1990).
3. R. K. Srivastava, P. A. Ramachandran and M. P. Dudukovic, Radiation view factors in Czochralski crystal growth apparatus for short crystals, *J. Crystal Growth* **74,** 281–291 (1986).
4. S. Miyahara, S. Kobayashi, T. Fujiwara, T. Kubo and H. Fujiwara, Global heat transfer model for Czochralski crystal growth based on diffuse-gray radiation, *J. Crystal Growth* **99,** 696–701 (1990).
5. L. J. Atherton, J. J. Derby and R. A. Brown, Radiative heat exchange in Czochralski crystal growth, *J. Crystal Growth* **84,** 57–78 (1987).
6. E. M. Sparrow and R. D. Cess, *Radiation Heat Transfer* (Augmented Edn), p. 145. McGraw-Hill, Washington, DC (1978).
7. H. Masuda, Analysis of radiation heat transfer among specularly and diffusely reflecting curved surfaces, *Japan Soc. Mech. Engrs, Ser.* II **44,** 2402–2410 (1978).
8. S. Maruyama and T. Aihara, Numerical analysis of radiative heat transfer from three dimensional bodies of arbitrary configurations, *JSME Int. J.* **30,** 1982–1987 (1987).
9. S. Maruyama, Radiation heat transfer between arbitrary three-dimensional bodies with specular and diffuse surfaces, *Numer. Heat Transfer, Part A* **24,** 181–196 (1993).
10. K. Yamamoto, Thermal conduction properties of the crystal and the melt silicon, *J. Japanese Assoc. Crystal Growth* **18,** 424–430 (1991).
11. S. Maruyama, Uniform isotropic emission from an involute reflector, *Trans. ASME, J. Heat Transfer* **115,** 492–495 (1993).
12. H. Hayasaka, K. Kudo, H. Taniguchi, I. Nakamachi, T. Omori and T. Katayama, Radiative heat transfer analysis by the radiative heat ray method, *Trans. Japan Soc. Mech. Engrs* **52,** 1734–1740 (1986).
13. J. R. Howell, *A Catalog of Radiation Configuration Factors*, p. 165. McGraw-Hill, Washington, DC (1982).
14. S. Maruyama and T. Aihara, Radiation heat transfer of arbitrary axisymmetric bodies with specular and diffuse surfaces, *Trans. Japan Soc. Mech. Engrs, Ser. B* **59,** 3202–3209 (1993).